

## **Primary measurement of massic activity of Am-241 by cryogenic decay energy spectrometry**

Ryan P. Fitzgerald, Bradley Alpert, Denis E. Bergeron, Max Carlson, Richard Essex, Sean Jollota, Kelsey Morgan, Shin Muramoto, Svetlana Nour, Galen O'Neil, Daniel R. Schmidt, Gordon Shaw, Daniel Swetz, and R. Michael Verkouteren

*National Institute of Standards and Technology, 100 Bureau Drive, Gaithersburg, MD USA*

### Keywords

radionuclide metrology; quantitative analysis; radioactivity; decay energy spectrometry; cryogenic calorimetry; inkjet gravimetry; transition edge sensor; TES

### Abstract

We demonstrate a method for radionuclide assay that is spectroscopic with 100 % counting efficiency for alpha decay. Advancing both cryogenic decay energy spectrometry (DES) and drop-on-demand inkjet metrology, a solution of Am-241 was assayed for massic activity (Bq/g) with a relative combined standard uncertainty less than 1 %. We implement live-timed counting, spectroscopic analysis, validation by liquid scintillation (LS) counting, and confirmation of quantitative solution transfer. Experimental DES spectra are well modeled with a Monte Carlo simulation. The model was further used to simulate Pu-238 and Pu-240 impurities, calculate detection limits, and demonstrate the potential for tracer-free multi-nuclide analysis, which will be valuable for new cancer therapeutics based on decay chains, Standard Reference Materials (SRMs) containing impurities, and more widely in nuclear energy, environmental monitoring, security, and forensics.

## 1. Introduction

We present a new spectroscopic capability for quantifying radionuclides in solution. Radionuclide standards must be based on primary reference measurements, meaning that the methods are internally consistent, self-calibrating, and not dependent on any measurement standard for a quantity (i.e., Bq) of the same kind [1]. Existing primary methods for radioactivity measurements are generally not spectroscopic, so are limited to single-radionuclide solutions and rely on secondary measurements by other methods to identify, quantify, and place limits on radionuclidic impurities that can cause bias in the primary measurement [2]. We demonstrate a new primary method for measuring activity of microgram quantities of samples that may contain multiple radionuclides, such as environmental samples, cancer therapeutics based on decay chains, and samples containing radionuclidic impurities. Here we perform a primary standardization of Am-241 massic activity and place limits on alpha-emitting impurities.

The new approach is based on quantum devices called transition-edge sensors (TES). The basic operational principle involves cooling an absorber to just below its superconducting transition temperature,  $T_C$ , so that minuscule amounts of absorbed energy result in a very large increase in electrical resistance [3]. In recent years, TESs have become familiar in multiple fields of science from space-based astronomy to laboratory atomic, ion, and plasma physics where they have radically improved sensitivity and resolution in x-ray spectroscopy [4]. Decay Energy Spectrometry (DES) using TES and other cryogenic sensors (such as magnetic microcalorimeters [MMCs]) has great potential for absolute activity measurements for alpha [5], beta [6], electron capture [7], and mixed decays [8], achieving spectral resolving powers of up to 5000 [9]. In DES, the energy of a single radioactive decay is captured in an absorber and measured with a TES. Because the total energy ( $Q$ ) of the nuclear decay is measured (in ideal cases), DES is sometimes referred to as  $Q$ -spec [9]. Among other efforts, a European consortium called Prima-LTD has achieved significant progress toward their stated goal of measuring absolute activity with low-temperature detectors [10].

Here, we report advances in DES measurements, pulse processing with live-timed spectroscopic analysis, and drop-on-demand inkjet gravimetry that enable a fully-realized DES-based standardization of an Am-241 solution for massic activity (Bq/g), achieving uncertainties that are competitive with established primary methods.

## 2. Method

### 2.1 Materials

The stock solution of Am-241 was in  $\approx 1$  mol/L nitric acid having nominal massic activity of  $1.5 \times 10^5$  Bq/g at the reference date 1 September 2022. Extremely small aliquots of solution ( $< 10$   $\mu$ g) were dispensed (Section 2.2) for cryogenic DES measurements (Section 2.3). Larger ( $\approx 50$  mg) aliquots were dispensed by traditional methods for validation measurements using non-spectroscopic liquid scintillation counting (Section 2.4).

For this first demonstration, Am-241 was chosen as it decays purely by alpha decay (rather than beta decay or electron capture), mostly to the ground state of Np-237 [11, 12]. The resulting alpha particle and Np-237 recoil nucleus come to rest in the gold absorber, depositing their kinetic energies. There is a significant alpha decay branch to an excited state of Np-237 that sometimes results in the emission of a low-energy ( $\approx 60$  keV) gamma ray that may be absorbed in the gold sample or may escape. This escape provides a useful test of our spectral analysis methods.

The Am-241 solution was deposited (Section 2.2) onto foils with nanoporous gold (npAu) surface films to create the DES sources. The npAu films had a thickness of  $(1.6 \pm 0.1)$   $\mu$ m, an average pore diameter of  $(44 \pm 13)$  nm, and a porosity of approximately 21 % (Figure 1). Volumetric solute transfer was confirmed by depositing an aqueous nitric acid solution containing 5  $\mu$ g/g CsNO<sub>3</sub>, followed by secondary ion mass spectrometry depth profiling to track the presence of Cs<sup>+</sup> ions as a function of film depth. The Cs was a non-radioactive surrogate for Am, and the concentration used was significantly higher to ensure detection using the technique.

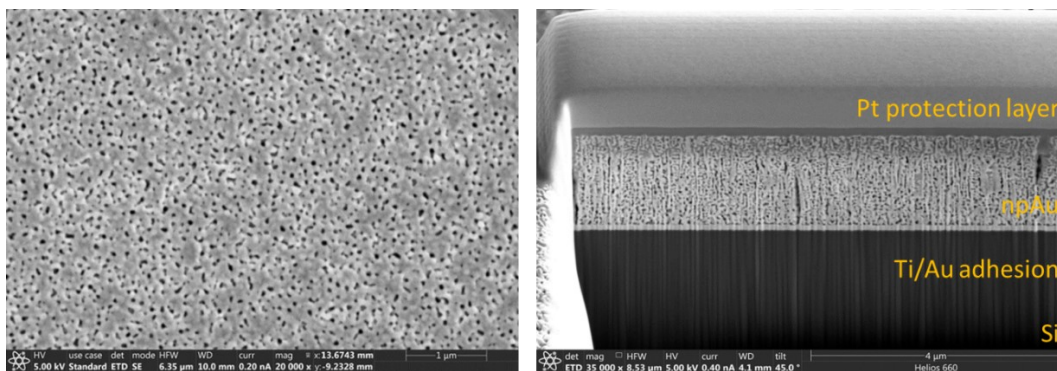


Figure 1. SEM images showing the surface structure of the nanoporous Au (npAu) film (left), and the cross section of the film after FIB cross sectioning (right). These npAu films ( $(1.6 \pm 0.1) \mu\text{m}$  in thickness) were deposited onto Si wafers to facilitate analysis using advanced surface analytical tools. Using the imaging software, the average diameter of the pores on the surface of the films were measured to be  $(44 \pm 13) \text{ nm}$  with a porosity of 21 %, while those from the cross section were  $(47 \pm 26) \text{ nm}$  and 18 %, respectively, and shows the uniformity of the porous structure.

Secondary ion mass spectrometry (SIMS) depth profiles were obtained using an IONTOF IV instrument (Münster, Germany) equipped with a 30 keV  $\text{Bi}^+$  liquid metal ion source for both analysis and sputtering. Depth profiling was performed in non-interlaced mode, where 50 scans of analysis in pulsed beam mode and 75 scans of sputtering in continuous beam mode are operated in separately per cycle, with both beams kept inside a  $(500 \times 500) \mu\text{m}$  area. The sputtering ion dose was  $3.6 \times 10^{15} \text{ ions/cm}^2$  at a current of 11.9 nA per cycle. To prevent pillar-like topography from changing the sputter rate, sample rotation was performed with the 6-axis stage equipped with the instrument and was rotated by  $90^\circ$  after every cycle [13]. Crater depth measurements were performed using the Dektak XT stylus profilometer (Bruker Corporation, Tucson, AZ) equipped with a  $2.5 \mu\text{m}$  radius stylus tip. A 2 mm line scan was used to ensure that a large enough region outside the crater was measured to provide sufficient area for leveling.

The distribution of the Cs was fairly uniform throughout the entire thickness of the film (Figure 2). The npAu films were subsequently cut into 2.4 mm squares using a laser cutter and cleaned again using nitric acid to eliminate ambient carbon contamination before inkjet deposition.

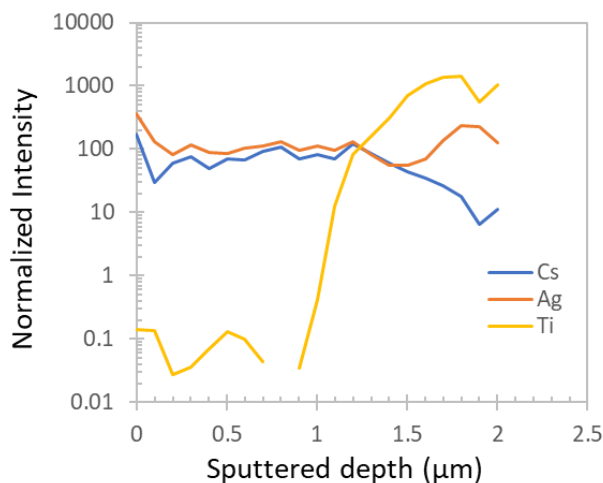


Figure 2. Secondary ion mass spectrometry (SIMS) depth profile showing the relative concentration of  $\text{Cs}^+$ ,  $\text{Ag}^+$ , and  $\text{Ti}^+$  ions inside the npAu film as a function of sputtered depth. The intensities were normalized to the  $\text{Au}^+$  ions to correct for the preferential sputtering effect at the initial transient region. Note that the intensity is plotted on a log scale, and the position of the Ti interface occurs around a depth of  $1.5 \mu\text{m}$  at 50% of the maximum intensity.

## 2.2 Gravimetric Inkjet Dispensing

Inkjet dispensing was performed using a metrology-level Jetlab 4 tabletop printer (Microfab Technologies, Plano, TX)\* that incorporates an ultramicrobalance to calibrate drop mass before and after dispensing onto the npAu DES substrates. Previous work at NIST has established procedures for measuring inkjet-dispensed masses with  $< 1\%$  relative combined standard uncertainty [14-16]. Both DES sources (0.01 mg to 0.1 mg) and liquid-scintillation (LS) sources (1 mg to 10 mg) were prepared by inkjet dispensing.

For the present work, additional steps were taken to mitigate evaporation effects on the measured dispensed mass. During mass calibration, the inkjet tip was lowered to a few mm above the

---

\* Certain commercial equipment, instruments, or materials are identified in this paper to foster understanding. Such identification does not imply recommendation by the National Institute of Standards and Technology, nor does it imply that the materials or equipment identified are necessarily the best available for the purpose.

surface of water contained in a gold-plated glass vessel with a ~2 mm diameter opening. Previous tests, performed at multiple heights above the liquid to estimate residual evaporation, allowed correction for evaporation-in-flight of droplets travelling to the balance vessel.

To check for evaporative changes in the concentration of the Am-241 solution in the inkjet reservoir, LS sources were prepared from the solution before and after preparation of the DES sources by both the traditional pycnometer method (larger masses) and by inkjet deposition [17]. These LS sources served as a radiometric confirmation of inkjet gravimetry.

To test for potential losses of radioactive material due to stray satellite droplets of solution or leakage from the foil, the “placemat” method described previously[18] was employed. Each of six gold foils was placed on a square of hydrogel during dispensing of larger ( $\approx 1$  mg, 16 000 drop, 160 Bq) aliquots of the Am-241 solution. (The foils for DES were also prepared over gel placemats, but the lower activities made detection of any stray material unlikely, so this dedicated study with higher activity was undertaken.) After the foil sources dried, each foil and gel were placed in their own LS vials and counted in two commercial liquid scintillation counters to test for any activity lost from the foil during dispensing or drying.

Following drying of the inkjet-deposited solution on the nanoporous surface of the foil, each foil was folded in half and rolled flat using a manual roller press to encapsulate the source material [19]. Each foil was then coated on one side with a thin layer of In-Ga eutectic for thermal contact and placed on the 2 mm by 1 mm gold-coated sample pad on a 5 mm by 5 mm TES chip.

### 2.3 Decay Energy Spectrometry

DES was performed using transition-edge sensors (TES) similar to those used for plutonium isotopic ratio studies [20]. Since the goal of this work is absolute massic activity of radionuclides that are generally well-separated in decay energy, the focus was on simple, quantitative source preparation, with modest (for cryogenic sensors) energy resolution of about 5 keV. A dilution refrigerator was used to maintain a base temperature of 50 mK. A total of 5 foil-encapsulated Am-241 sources and 2 blank foils, mounted on the sample pads of TES chips, were measured on multiple occasions. Each chip was voltage-biased to 20 % of the TES normal resistance. Data were acquired with commercial SQUID (superconducting quantum interference device)

amplifiers and analog-to-digital converters (ADCs). Continuous signals were recorded at a sample rate of  $10^5 \text{ s}^{-1}$ .

Typical pulses had rise times of 0.2 ms and fall times of 25 ms. Pulse processing consisted of a live-timed [21-23] counting algorithm that required an absence of triggers within a fixed time before a pulse (traditional live-timing using extending, or paralyzable, dead time [24]) and after a pulse (to ensure clean pulses for spectrometry) for the time to be considered live. The imposed dead-time was chosen to be longer than any inherent trigger dead-time of the system and to avoid nonlinearity of closely piled up pulses.

The offline pulse processing implementation followed a series of steps: 1) convolve the data with a “trigger filter”; 2) note the location of local maxima in the output of 1 as trigger times; 3) choose pulses with sufficient time after the previous trigger (imposed deadtime A) and time until the next trigger (imposed deadtime B); 4) apply a filter to each pulse to extract a pulse height; 5) apply a linear calibration based on the clear Am-241 Q peak. A subset (about 0.3 %) of pulses was identified where a gamma ray escaping from the npAu foil interacts with the rest of the TES directly; these pulses have a faster-rising edge and a larger proportion of the total pulse area in the first 1 ms of the data. The spectroscopic information from these pulses is vastly reduced; since the only  $\gamma$ -ray emitting radionuclide identified in this sample was Am-241, those events can be assigned as Am-241 decays. In measurements with multiple nuclides, these pulses will not be so easily accounted for, so we intend to alter the TES design to reduce the rate of these interactions by at least 10x.

The live time for each pulse included in the final histogram is calculated as the time from the trigger before to the trigger after minus the imposed deadtimes A and B. The live time for the final histogram is the sum of live times for all pulses included in the histogram. The activity in a given region of interest (ROI) is the sum of counts in that ROI divided by the live time of the histogram.

To check that there were no hidden dead-times or double triggering, a histogram of arrival time differences between subsequent triggers (Figure 3) was created. The data follow the expected exponential distribution for random radioactive decay events.

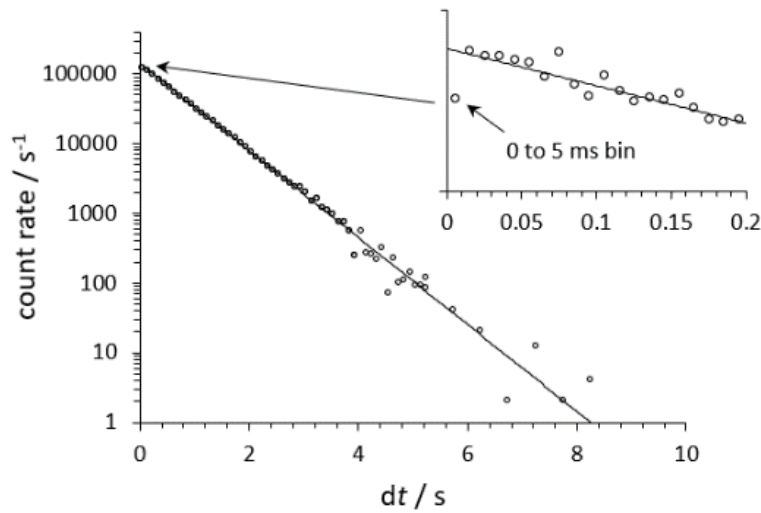


Figure 3. Histogram of arrival time difference between subsequent pulse triggers. Inset shows that the expected linear trend (on log scale) holds down to  $< 5$  ms, limited by the trigger filter and pulse rise time. The live-timed counting method used extending deadtimes much longer than 5 ms (typically 200 ms) to ensure accurate absolute counting.

In addition, pulses were classified by shape, which indicates when a  $\gamma$ -ray (either from the source or background) interacts with the chip without thermalization in the source foil. These interactions produce fast pulses that can be distinguished from pulses originating in the source, further reducing background in the low-energy portion of the spectrum.

The resulting DES spectrum was compared to Geant4 [25] Monte Carlo simulations to search for any radioactive impurities within the Am-241 energy region of interest (ROI) shown in Figure 4. As no impurities were found, the Am-241 count rate was taken as the sum of live counts in the Am-241 ROI divided by the live time. Had impurities been present, the impurity spectrum could be fit using the Monte Carlo to subtract its contribution to the ROI.



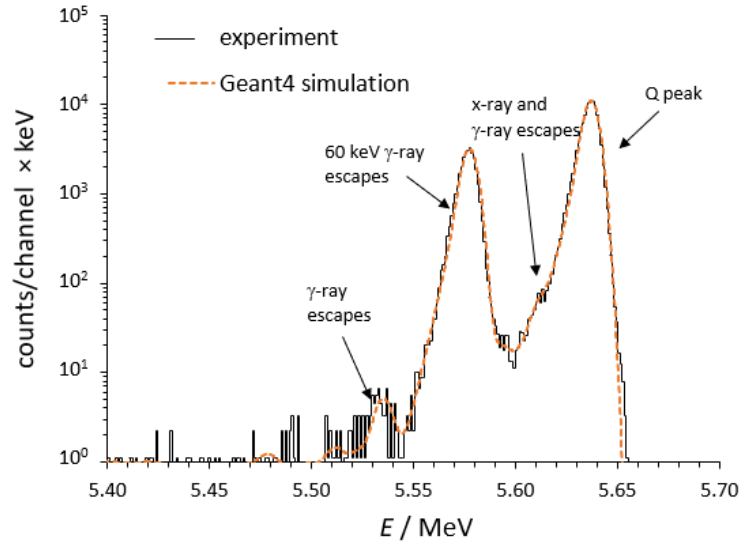


Figure 4. Experimental Am-241 spectrum (25  $\mu\text{m}$  foil; 45 h measurement) with Geant4 simulation fit (Gaussian width and left exponential tail as free parameters, applied to the whole spectrum). The Am-241 decay energy, Q, and escape peaks from  $\gamma$  rays and x rays are indicated.

## 2.4 Validation measurements

The Am-241 solution was assayed for massic activity of Am-241 before and after the DES experiment using well-established non-spectroscopic primary methods based on  $4\pi\alpha$  liquid scintillation (LS) counting. LS counting was carried out on commercial instruments and on a custom-built three photomultiplier tube counter (often referred to as a “TDCR system”, even when the triple-to-double coincidence ratio method is not employed) [26].  $\gamma$ -ray spectrometry [27] measurements were performed to check for photon-emitting radionuclide impurities.

LS sources were measured in two commercial counters, one operated with an open energy window for absolute counting and one operated in a low-background mode, and in a custom-built TDCR system [26]. The low-background instrument, featuring alpha-beta discrimination, was used primarily for the placemat measurements, due to its high sensitivity. The open-window counter was used to confirm the Am-241 massic activity before and after the inkjet dispensing of DES sources to validate that the massic activity did not change (e.g., due to evaporation in the inkjet reservoir).  $4\pi$  LS counting is a well-established method for non-spectroscopic primary

standardization of activity when the nuclide and purity of a sample is known and was used for live-timed absolute counting [26, 28].

### 3. Results

#### 3.1 Background and impurities

Two blank foils were measured for 40 000 s and 160 000 s, with 1 count and 0 counts above 0.5 MeV, respectively, corresponding to negligible background for Am-241 (Figure 5). The trigger threshold was set based on signal-to-noise for each spectrum, corresponding to about 15 keV. No evidence of Pu-241 decay (beta endpoint 20.5 keV) was seen. The beta background rate was about  $6 \cdot 10^{-4} \text{ s}^{-1}$ , which is about  $10^4 \times$  lower than that for LS. Gamma-ray spectrometry measurements were carried out for 70 hours and no impurities were found. The most likely impurities (Pu isotopes) produce few to no  $\gamma$ -rays, so the DES spectra provide a stronger impurity constraint.

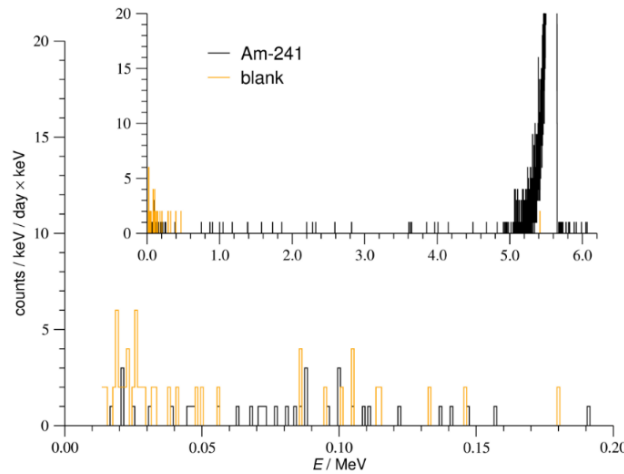


Figure 5. DES spectra for an Am-241 source and for a blank foil measured concurrently on separate TES chips. The noise cutoffs are about 10 keV and 15 keV for the Am-241 and blank, respectively. No evidence of Pu-241 (20.5 keV endpoint) is seen. The count rate between 20 keV and 200 keV was  $(4.7 \pm 0.8) \cdot 10^{-4} \text{ s}^{-1}$  and  $(6.8 \pm 1.3) \cdot 10^{-4} \text{ s}^{-1}$  for the Am-241 and blank, respectively, indicating no beta-particle emitting impurities in that region. In the Am-241 region, there was 1 count in 43000 s of measurement time for the blank, with a

rate  $(2.4 \pm 0.2) \cdot 10^{-5} \text{ s}^{-1}$ . A second blank was run for longer with no counts, giving an upper limit of  $\approx 6 \cdot 10^{-6} \text{ s}^{-1}$ .

The resolving power for DES was about  $150\times$  that for LS, allowing for detection of potential radionuclide impurities by DES (Figure 6). Figure 7 shows simulated spectra containing Pu-240 and Pu-238 impurities at activity ratios relative to Am-241 of 0.02 % and 0.15 %, respectively. The spectral evidence of these low-level impurities illustrates the value of this spectroscopic method for, e.g., characterizing Standard Reference Materials (SRM), which typically have uncertainties  $> 0.15 \%$ . No evidence of low-energy beta decays from Pu-241 was observed, though the trigger threshold is near the endpoint energy.

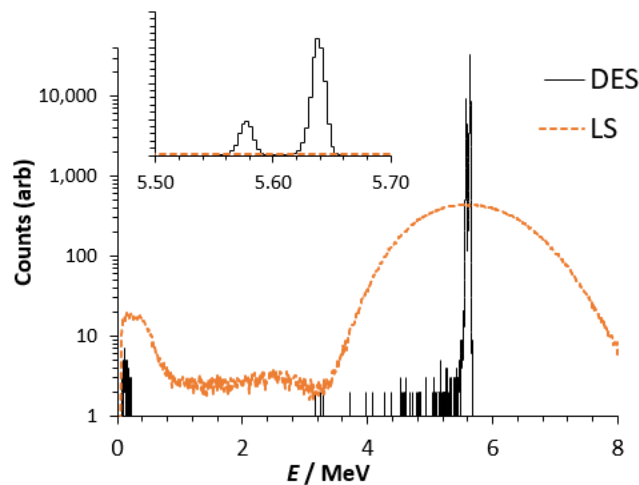


Figure 6. Comparison of DES and LS spectra for Am-241. (Note log scale vertical scale, linear on inset). Both detectors have  $\approx 100 \%$  counting efficiency, but DES has much higher energy resolution. Note, the LS detector response is highly non-linear and differs for alphas, betas, and gammas. Here the bin energies have been scaled linearly to align the alpha peak to 5.6 MeV. The two spectra are scaled to contain the same integral number of counts in the spectrum. No background subtraction has been made, such that low-energy background is present (also seen in blank samples).

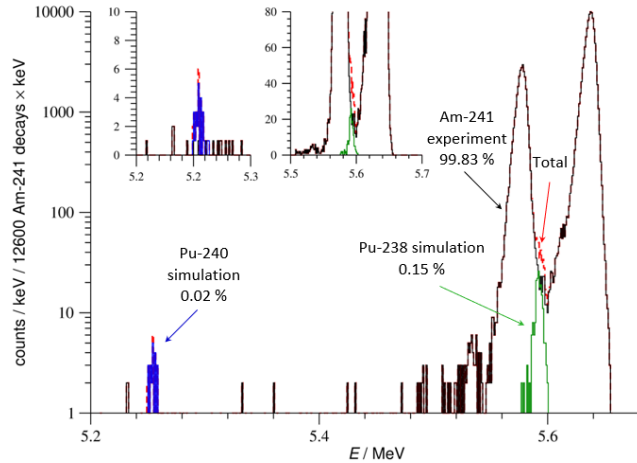


Figure 7. Impurity search: Same experimental Am-241 spectrum from Figure 2 (black  $\approx 126,000$  counts) with the addition of Geant4 simulated impurities of Pu-240 (25 counts, or 0.02 % of total) and Pu-238 (189 counts, or 0.15 % of total) to illustrate detectability in the composite spectrum (red line). No evidence of radionuclide impurities was found in the experimental spectrum.

### 3.2 Placemat study

The average and standard deviation of the distribution of the relative activity on the placemats vs. foils for the 6 sources was  $(0.017 \pm 0.018)$  % (Figure 8). The highest value was 0.053 %, which is a  $5\times$  improvement over the earlier hand-dispensed microdrop method [18]. Based on these results, a conservative uncertainty of 0.05 % was assumed due to material loss during the quantitative source preparation for the DES measurements.

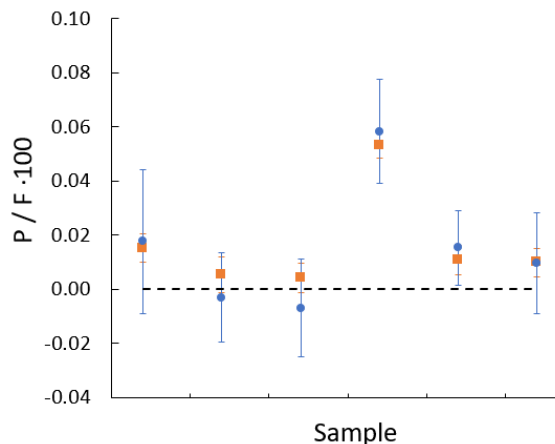


Figure 8. Results of placemat test showing the ratio of (background-subtracted) counts on the placemat ( $P$ ) to that on the foil ( $F$ ), as measured in two different LS counters. For the low background LS counter (orange squares), the statistical uncertainty on the net count rate ( $P$ ) for the placemats was about  $0.004 \text{ s}^{-1}$ , or  $0.002 \%$  of the foil count rate ( $F$ ). The relative loss  $P/F$  average and standard deviation of the distribution for the 6 sources was  $(0.017 \pm 0.018) \%$ . The highest value was  $0.053 \%$ , which is a 5 times improvement over the earlier hand-dispensed microdrop method.

### 3.3 Massic activity

The weighted average activity for 4 DES sources was  $(1.357 \pm 0.007) \text{ Bq}$ , which combined with the dispensed mass from the inkjet, gives a massic activity of  $145.7 \text{ kBq/g}$  with relative combined standard uncertainty  $u_c = 0.72 \%$  (Table 1). The first DES source in the series gave a positively biased activity that is explained by a concentrating "first aliquot effect" observed previously. We have investigated this effect further in a series of follow-up experiments, but in the present work, to avoid uncertainties introduced by any correction, the first sample was simply excluded from the massic activity analysis. The major sources of uncertainty were counting statistics and the uncertainty in the dispensed mass. The relative counting statistics uncertainty ( $0.49 \%$ ) was taken as the uncertainty in the weighted mean count rate for 4 identical Am-241 samples (same number of drops of active solution), where each individual mean uncertainty was the square root of the number of counts in the ROI. For comparison, the "external uncertainty," calculated as the weighted standard deviation for the 4 sources was  $0.36 \%$ , indicating that the

sources were statistically identical. The source mass uncertainty was primarily due to the calibration of the mass per drop from the inkjet [14].

Table 1. Uncertainty analysis for DES massic activity measurement where  $u_i$  are the relative uncertainty in the final massic activity of the solution due to each of the input quantities. The  $u_i$  values are added in quadrature to determine  $u_c$  [29].

Component	$u_i$ (%)
Counting statistics	0.49
Live time	0.10
Background	0.00
Pulse assignment	0.06
Mass	0.51
Limit on material loss	0.05
Limit on impurities	0.05
$u_c$ (%)	<b>0.72</b>

The standard LS value taken for the massic activity was that of the TDCR system for 5 LS sources prepared by pycnometer, with an average massic activity of 144.85 kBq/g and  $u_c = 0.33$  %. All of the LS and DES measurements resulted in consistent massic activities for the solution (Figure 9). No change in massic activity was observed during the experiment from evaporation or other effects.

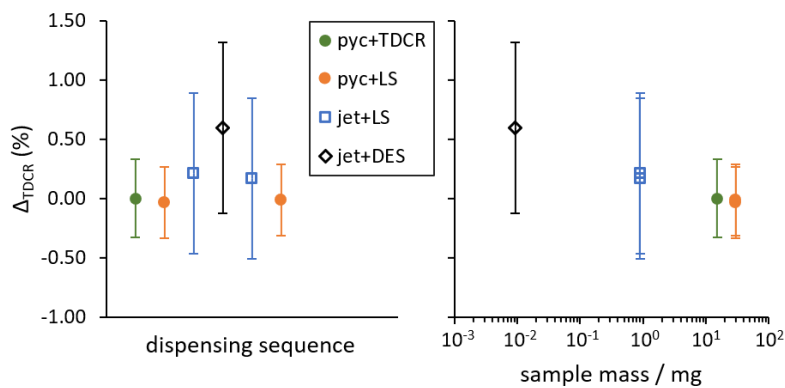


Figure 9. Relative difference  $\Delta_{TDCR}$  of massic activity from the average of the standard method (pycnometer + TDCR). Bars are combined standard uncertainties on each measurement method. **Left:** results plotted in time order of source

dispensing; no change in massic activity from evaporation or other effects was observed over time. **Right:** results plotted against aliquot mass per sample to highlight the good agreement even for very small sample masses achievable by DES.

#### 4. Discussion

In this work we successfully quantify Am-241 massic activity while spectrally excluding the presence of the nearby Pu-240 and Pu-238 isotopes at the 0.02 % to 0.15 % level. Geant4-based radiation transport simulation results validate understanding of the DES and predict sensitivity to these radioactive impurities. These impurities are invisible to  $\gamma$ -ray spectrometry because they do not emit photons and would require chemical processing to detect by traditional alpha spectrometry. Further, since Pu-241 and Am-241 are isobars, they can interfere in mass spectrometry but are readily resolved by DES (decay energies of 21 keV and 5637 keV, respectively). This capability enables primary measurement of activity for multiple radionuclides in one assay on drop-dried sources, without the need for chemical processing and the attendant chemical tracers.

Liberation from chemical separations and efficiency tracers brings benefits beyond faster throughput and lower cost. In traditional methods, major sources of uncertainty in the massic activity measurement include chemical separation and detection efficiency, along with ambiguities from spectral interferences from isotopic impurities. For example, recent measurements of a Pa-231 solution had a goal of < 0.2 % uncertainty, but the results had uncertainty > 3 % due to these issues [30]. If DES were applied to this case, sources would be made and counted with 100 % efficiency and spectral resolution would cleanly separate Pa-231 from an Ac-227 impurity, resulting in predicted uncertainties within the goal.

#### 5. Conclusion

The state-of-the-art DES measurements reported here are quantitative in activity and spectroscopic, enabling a new capability of multi-nuclide absolute activity. Through inkjet gravimetry, DES sources have been prepared with precise and radiometrically validated links to a stock solution. This paper thus presents a DES-determined massic activity, validated with

another primary method and achieving relative combined standard uncertainties that are competitive with mature techniques in radionuclide metrology.

Longer measurements and higher count rates can be employed to reduce statistical uncertainties. With a TES optimized for higher heat flow, the activity per source could be increased, resulting in lower counting uncertainties. In future quantitative DES work, the energy resolution, which is important to the sensitivity to both alpha and beta impurities, may be improved by 4× or more based on the highest resolution DES results in the literature [9].

Efforts are underway to decrease the uncertainty in sample mass using a new balance being developed at NIST. This device incorporates the dispenser into the balance itself and realizes mass traceable directly to electrical measurements. For 1 mg masses of gravimetrically diluted solution, expected uncertainties are of order 0.1 % [31].

## 6. Acknowledgements

The authors acknowledge Mark Croce and Katherine Schreiber of Los Alamos National Laboratory and Geon-Bo Kim of Lawrence Livermore National Laboratory for sharing source preparation methods. RF acknowledges the NIST Radiation Physics Building modernization team for their support.

## 7. References

- [1] BIPM, I., IFCC, ILAC, ISO, IUPAC, IUPAP and OIML, *International vocabulary of metrology -- Basic and general concepts and associated terms (VIM)*. 2012, JCGM.
- [2] Collé, R., *Radionuclidic standardization by primary methods: An overview*. Journal of Radioanalytical and Nuclear Chemistry, 2009. **280**(2): p. 265-273.
- [3] Irwin, K.D. and G.C. Hilton, *Transition Edge Sensors*. 2005, Heidelberg: Springer.
- [4] Morgan, K.M., *Hot science with cool sensors*. Physics Today, 2018. **71**(8): p. 28-34.
- [5] Kim, G.B., et al., *Absolute Decay Counting of <sup>146</sup>Sm and <sup>147</sup>Sm for Early Solar System Chronology*. Journal of Low Temperature Physics, 2022. **209**(5-6): p. 824-831.
- [6] Loidl, M., et al., *Beta spectrometry with metallic magnetic calorimeters in the framework of the European EMPIR project MetroBeta*. Applied Radiation and Isotopes, 2019. **153**.
- [7] Croce, M.P., et al., *Development of Holmium-163 Electron-Capture Spectroscopy with Transition-Edge Sensors*. Journal of Low Temperature Physics, 2016. **184**(3-4): p. 958-968.
- [8] Tollefson, A.D., et al., *Measurement of (227)Ac impurity in (225)Ac using decay energy spectroscopy*. Appl Radiat Isot, 2021. **172**: p. 109693.
- [9] Koehler, K.E., *Low Temperature Microcalorimeters for Decay Energy Spectroscopy*. Applied Sciences, 2021. **11**(9).



- [10] Naehle, O.e.a., *Publishable Summary for 20FUN04 PrimA-LTD Towards new primary activity tandardisation methods based on low-temperature detectors*. 2023.
- [11] Bé, M.-M.C., V.; Dulieu, C.; Mougeot, X.; Browne, E.; Chechev, V.; Kuzmenko, N.; Kondev, F.; Luca, A.; Galán, M.; Arinc, A.; Huang, X., *Table of Radionuclides*, in *BIPM Monographie*. 2010: Sévres.
- [12] Chechev, V.P. and K.N. Kuzmenko. *DDEP Evaluation of Am-241*. Atomic and Nuclear data 2010 [cited 2024; Available from: [http://www.lnhb.fr/nuclides/Am-241\\_tables.pdf](http://www.lnhb.fr/nuclides/Am-241_tables.pdf)].
- [13] Muramoto, S. and D. Graham, *Deep depth profiling using gas cluster secondary ion mass spectrometry: Micrometer topography development and effects on depth resolution*. Surf Interface Anal, 2021. **53**(9): p. 814-823.
- [14] Elliott, L.C.C., et al., *Sub-picoliter Traceability of Microdroplet Gravimetry and Microscopy*. Analytical Chemistry, 2022. **94**(2): p. 678-686.
- [15] Essex, R.M., et al., *Isotope dilution mass spectrometry as an independent assessment method for mass measurements of milligram quantities of aqueous solution*. International Journal of Mass Spectrometry, 2023. **483**: p. 116969.
- [16] Verkouteren, R.M. and J.R. Verkouteren, *Inkjet metrology II: resolved effects of ejection frequency, fluidic pressure, and droplet number on reproducible drop-on-demand dispensing*. Langmuir, 2011. **27**(15): p. 9644-53.
- [17] Sibbens, G. and T. Altitzoglou, *Preparation of radioactive sources for radionuclide metrology*. Metrologia, 2007. **44**(4): p. S71-S78.
- [18] Bergeron, D.E., et al., *Gravimetric deposition of microliter drops with radiometric confirmation*. Applied Radiation and Isotopes, 2023. **201**: p. 111025.
- [19] Jang, Y.S., et al., *Development of Decay Energy Spectroscopy for Radionuclide Analysis Using Cryogenic  $4\pi$  Measurements*. Journal of Low Temperature Physics, 2012. **167**(5-6): p. 967-972.
- [20] Hoover, A.S., et al., *Measurement of the  $^{240}\text{Pu}/^{239}\text{Pu}$  mass ratio using a transition-edge-sensor microcalorimeter for total decay energy spectroscopy*. Anal Chem, 2015. **87**(7): p. 3996-4000.
- [21] Pomme, S., R. Fitzgerald, and J. Keightley, *Uncertainty of nuclear counting*. Metrologia, 2015. **52**(3): p. S3-S17.
- [22] Baerg, A.P.M., K.; Bowes, G.C., *Live-timed anti-coincidence counting with extending dead-time circuitry*. Metrologia, 1976. **12**: p. 77-80.
- [23] Bouchard, J., *MTR2: a discriminator and dead-time module used in counting systems*. Applied Radiation and Isotopes, 2000. **52**: p. 441-446.
- [24] Knoll, G.F., *Radiation Detection and Measurement*. 2010: Wiley.
- [25] Agostinelli, S., et al., *Geant4—a simulation toolkit*. Nuclear Instruments and Methods in Physics Research Section A: Accelerators, Spectrometers, Detectors and Associated Equipment, 2003. **506**(3): p. 250-303.
- [26] Zimmerman, B.E., R. Colle, and J.T. Cessna, *Construction and implementation of the NIST triple-to-double coincidence ratio (TDCR) spectrometer*. Appl Radiat Isot, 2004. **60**(2-4): p. 433-8.
- [27] Pibida, L., et al., *Software studies for germanium detectors data analysis*. Appl Radiat Isot, 2006. **64**(10-11): p. 1313-8.
- [28] Broda, R., P. Cassette, and K. Kossert, *Radionuclide metrology using liquid scintillation counting*. Metrologia, 2007. **44**(4): p. S36-S52.
- [29] BIPM, et al., *Evaluation of measurement data -Guide to the expression of uncertainty in measurement*. JCGM, 2008.
- [30] Essex, R.M., et al., *Preparation and calibration of a 231 Pa reference material*. Journal of radioanalytical and nuclear chemistry, 2019. **322**(3): p. 1593-1604.
- [31] Schulze, S., et al., *Development of a High Precision Electrostatic Force Balance for Measuring Quantity of Dispensed Fluid as a New Calibration Standard for the Becquerel*. Measurement Science and Technology, 2024.

